International Journal of Biological Macromolecules 180 (2021) 729–738

Contents lists available at ScienceDirect

International Journal of Biological Macromolecules

journal homepage: http://www.elsevier.com/locate/ijbiomac

Glucuronoxylan-based quince seed hydrogel: A promising scaffold for tissue engineering applications

Meltem Guzelgulgen [a], Dilce Ozkendir-Inanc [b], Umit Hakan Yildiz [c,d,*], Ahu Arslan-Yildiz [a,*]

[a] Department of Bioengineering, Izmir Institute of Technology (IZTECH), 35430 Izmir, Turkey
[b] Department of Photonic, Izmir Institute of Technology (IZTECH), 35430 Izmir, Turkey
[c] Department of Chemistry, Izmir Institute of Technology (IZTECH), 35430 Izmir, Turkey
[d] Department of Polymer Science and Engineering, Izmir Institute of Technology (IZTECH), 35430 Izmir, Turkey

ARTICLE INFO

Article history:
Received 22 December 2020
Received in revised form 14 March 2021
Accepted 17 March 2021
Available online 21 March 2021

Keywords:
Quince seed hydrogel
Hydrocolloid
3D cell culture
Tissue engineering
Polysaccharide hydrogel
Scaffold

ABSTRACT

Natural gums and mucilages from plant-derived polysaccharides are potential candidates for a tissue-engineering scaffold by their ability of gelation and biocompatibility. Herein, we utilized Glucuronoxylan-based quince seed hydrogel (QSH) as a scaffold for tissue engineering applications. Optimization of QSH gelation was conducted by varying QSH and crosslinker glutaraldehyde (GTA) concentrations. Structural characterization of QSH was done by Fourier Transform Infrared Spectroscopy (FTIR). Furthermore, morphological and mechanical investigation of QSH was performed by Scanning Electron Microscopy (SEM) and Atomic Force Microscopy (AFM). The protein adsorption test revealed the suitability of QSH for cell attachment. Biocompatibility of QSH was confirmed by culturing NIH-3T3 mouse fibroblast cells on it. Cell viability and proliferation results revealed that optimum parameters for cell viability were 2 mg mL^{-1} of QSH and 0.03 M GTA. SEM and DAPI staining results indicated the formation of spheroids with a diameter of approximately 300 μm. Furthermore, formation of extracellular matrix (ECM) microenvironment was confirmed with the Collagen Type-I staining. Here, it was demonstrated that the fabricated QSH is a promising scaffold for 3D cell culture and tissue engineering applications provided by its highly porous structure, remarkable swelling capacity and high biocompatibility.

1. Introduction

In recent years, hydrogels emerged as promising scaffold materials in 3D cell culture and tissue engineering field, since they are closely mimicking ECM structure and function [1–3]. Both natural and synthetic polymers have been developed and used in tissue engineering applications [1,4–9]. However synthetic polymers often exhibit toxic and non-biocompatible properties, while natural polymers provide more suitable microenvironment for cellular studies [5,10]. Polysaccharides are one of the biggest clusters of natural polymers and an example of natural polymers with the hydrogel forming ability. They are widely used in food industry [11–13] as; gelling agents, stabilizers, emulsifiers, thickeners, and in medical/pharmaceutical industry [14–16] as; gelling agents, coatings, biofilms, and as a wound dressing. Their biocompatibility, biological activity, biodegradability, and hydrogel forming ability make them a valuable biomaterial for tissue engineering [5,17–19]. Alginate [20], cellulose [21], hyaluronic acid [22], chitosan [23], xanthan gum [15], guar gum [15], carrageenan [5,15], dextran [15], and gellan gum [15,17] are the most abundant polysaccharide types that are used as a scaffold in tissue engineering.

Plants seeds are one of the most common sources of plant-based polysaccharides. They contain high-molecular weight polysaccharides that form hydrocolloids [24,25], which are usually water-soluble. Gelation ability makes hydrocolloids suitable materials for varied applications in food, pharmaceutical, and medical industry. As biomaterials, hydrocolloids demonstrate excellent properties such as; high swelling capacity, bioactivity, biocompatibility, biodegradability, having antioxidant and anti-inflammatory features [15]. Quince (*Rosaceae family*) is a small, yellow fruit that is native to West Asia and Middle East regions, and it has been heavily used in traditional medicine as well as in pharmaceutical industry. Quince seed is an important source of hydrocolloid/hydrogel that is composed of mostly cellulose and hydrolysable polysaccharides such as glucuronoxylan [26–28], unsaturated fatty acids [29] and amino acids [29]. Quince seed hydrocolloid is richer in terms of polysaccharide content and has a higher molecular weight [11] than other commercial hydrocolloids like gellan gum [30], xanthan gum [31], guar gum [32], and locust bean gum [33]. Polysaccharide-rich QSH has outstanding mechanical and biological properties that make it

* Corresponding authors.
E-mail addresses: meltemguzelgulgen@iyte.edu.tr (M. Guzelgulgen), dilceozkendir@iyte.edu.tr (D. Ozkendir-Inanc), hakanyildiz@iyte.edu.tr (U.H. Yildiz), ahuarslan@iyte.edu.tr (A. Arslan-Yildiz).

https://doi.org/10.1016/j.ijbiomac.2021.03.096
0141-8130/

a valuable and potential source as a biomaterial for medical applications. Although there are numerous studies on structural, physicochemical and mechanical properties of QSH [11,24,34], it's potential as a biomaterial has been under-evaluated and it has not been utilized in tissue engineering yet.

In this study, we aim to demonstrate the potential of QSH as a novel scaffold for tissue engineering application. For this aim, the gelation capacity of water-extracted QSH and its crosslinking ability with GTA was investigated. Chemical, structural and morphological characterization of QSH was done through ATR-FTIR, SEM and AFM analysis, respectively. Furthermore, cytotoxicity, cell viability, and proliferation were investigated through NIH-3T3 fibroblast cell culture to evaluate biocompatibility of QSH. We demonstrated the potential of QSH as a scaffold for 3D cell culture and tissue engineering applications.

2. Materials and methods

2.1. Preparation and gelation optimization of QSH

The QSH was prepared based on previous reports [25–29,34,35] with some modifications. Quince fruits from Izmir/Turkey were used, and seeds were separated from fresh fruits. Quince seeds were dried at room temperature approximately for a week. Dried seeds were gently crashed; white colored inner side of the seeds were removed with the help of forceps and brown colored outer shells of seeds were collected for further gelation process. Outer shells of seeds were mixed with ultra-pure water (UP H_2O) to obtain varying concentrations of QSH (1, 1.5, 2, 3.3, 5, and 10 mg/mL). After 24-h incubation at room temperature, QSH samples were filtered through gauze dressing and were lyophilized for approximately 72 h. Lyophilized QSHs were subsequently crosslinked by GTA. Either 0.03 M GTA for lightly-crosslinked QSH or 0.5 M GTA for heavily-crosslinked QSH, were prepared in acetone containing 0.05 M hydrochloric acid (HCl), and were incubated for 30 min at room temperature. Crosslinked QSHs were rinsed with UP H_2O for 3 times prior to further experiments, and kept lyophilized for long-term if not used directly after production.

2.2. Characterization of QSH scaffold

All characterization experiments were carried out by using non-crosslinked, lightly crosslinked (0.03 M GTA) and heavily crosslinked (0.5 M GTA) 2 mg mL^{-1} QSHs. Morphological characterization of QSH was accomplished with macro imaging, SEM analyses and pore size/pore distribution analyses. Scanning Electron Microscope (FEI QUANTA, 250 FEG) was used for SEM measurements. Lyophilized QSH samples were used for SEM analysis [13]. Average pore size and pore size distribution were determined via analysis of SEM images [36] by ImageJ image processing software (NIH) and OriginPro software (Northampton, MA).

Chemical characterization of QSHs was done with FTIR analysis in ATR mode (PerkinElmer, USA) from 1000 to 4000 cm^{-1} to identify the crosslinking of QSH. FTIR data was plotted and analyzed by OriginPro software (Northampton, MA).

Mechanical characterization of QSH was performed with AFM analysis. Surface topography and force-distance profiles of QSHs were obtained using the CoreAFM System (Nanosurf CoreAFM, Switzerland). Homogeneous and lyophilized QSH was placed on the microscope slide and tested in the AFM with beam shaped cantilever in contact mode (Stad 0.2 LAuD, NanoAndMore GMBH, Germany) having a nominal spring constant of 0.2 N nm^{-1} and tip radius of 7 nm. 512 lines at a speed of 2 s per line and 55 nN set point were acquired for each image. Root mean square (RMS) roughness and Young's Modulus values were calculated using the open-source software for SPM data analysis Gwyddion, Version 2.45. A series of 256 force-distance curves were calculated for 50 × 50 μm^2 regions and fit up to 1 μm tip deflections with a Hertz (sphere) model. Samples were indented at rates of approximately 1 μm s^{-1}, which is generally enough to explore elastic properties rather than viscoelastic properties of cells, matrix, or substrates.

The swelling ratio of QSH was analyzed through phosphate buffered saline (PBS) retention behavior. Crosslinked and lyophilized QSHs were measured to obtain dry weight (W_d) prior to immersing in 1× PBS solution at 37 °C, and then swollen weight (W_s) was observed at 1, 2, 4, 6, 8 and 24h. Excess PBS was removed from sample surface with the help of a filter paper. Swelling ratio was calculated by using $((W_s - W_d) / W_d) \times 100$ equation according to the literature [37,38], where W_s is swollen and W_d is dry weight of QSH. The data was analyzed by OriginPro software (Northampton, MA).

BCA Protein Assay (Pierce, Thermo Scientific) was used to analyze total protein adsorption on QSH scaffolds [39]. Lightly crosslinked and lyophilized QSHs were screened against bovine serum albumin (BSA) protein solutions with concentrations ranging from 0 μg mL^{-1} to 2000 μg mL^{-1}. After 2 h of incubation at 37 °C, QSHs were rinsed 3 times with PBS and transferred into 5% (w/v) sodium dodecyl sulfate (SDS) to solubilize adsorbed protein from scaffold surface. Absorbance was measured at 562 nm. Adsorbed and solubilized protein concentrations were quantified through BSA standard curve by OriginPro software (Northampton, MA).

2.3. 3D cell culture, viability and proliferation analysis

Mouse embryonic fibroblast cell line; NIH/3T3 (ATCC® CRL-1658™), which is one of the most widely utilized cell line for biomaterial development studies, was used as a model for cell culture assays [39]. Cells were maintained in growth medium containing 10% fetal bovine serum (FBS) (Gibco™, 10270) and 1% Penicillin-Streptomycin (Sigma-Aldrich, P4333) solutions in Dulbecco's Modified Eagle's medium (DMEM), High Glucose (Gibco™, 11965) and incubated at 5% CO_2, 37 °C. Lightly crosslinked and heavily crosslinked QSH scaffolds were analyzed to investigate the effects of GTA on cell viability and toxicity. After crosslinking, QSH scaffolds were rinsed 3 times with UP H_2O to eliminate GTA residues. Prior to cell culturing, crosslinked QSHs were sterilized through UV sterilization and then transferred to 48 well plates with DMEM complete medium (with 10% FBS and 3% Penicillin-Streptomycin) for conditioning.

AlamarBlue assay was used for cell viability and proliferation analysis. Low density (2×10^5) and high density (2×10^6) NIH 3T3 cells were seeded on QSHs for cell number optimization. Cells were cultured for up to 7 and 14 days to monitor short and long term cellular behaviors. Before analysis, scaffolds were transferred to fresh DMEM that contains resazurin sodium salt (%0.01 (v/v)) and incubated for 4 h. Absorbance values were obtained at 570 and 600 nm by microplate reader (Thermo Fisher Scientific Multiskan™ GO Microplate Spectrophotometer). Viability results were quantified by OriginPro software (Northampton, MA). Live/Dead assay was used to analyze toxicity of GTA on 3D cell cultures. High density (2×10^6) NIH 3T3 cells were seeded on QSHs for Live/Dead assay and cultured 1, 3 and 7 days. An equal volume of CytoCalcein and Propidium Iodide were mixed in buffer solution and applied to QSH scaffolds at 1, 3 and 7 days of 3D cell culture. Then samples were observed under the fluorescent microscope (Zeiss Observer Z1). As a control group TCPS (tissue culture polystyrene) was utilized. All cellular analyses were done by using 6 independent experimental data sets.

2.4. Cellular imaging

Morphological analysis of cellular spheroids was performed by SEM imaging. High density (2×10^6) NIH 3T3 cells were seeded on QSHs and cells were cultured on 48-well plates for up to 2 months to monitor ECM secretion. Cell cultured QSH scaffolds were first rinsed with 1× PBS

to eliminate cell culture medium and unwanted residues, and then they were fixed in 4% paraformaldehyde solution. After fixation, scaffolds were rinsed with 1× PBS and UP H_2O. Scaffolds were gold-coated prior to SEM analysis and were analyzed by SEM (FEI QUANTA, 250 FEG).

On the other hand, ECM formation and structural integrity were confirmed via Collagen and DAPI staining. Anti-collagen Type-I FITC (Milli-Mark™, FCMAB412F) was used for Collagen Type-I and DAPI (Sigma-Aldrich, D9542) was used for nucleus staining. QSH scaffolds were fixed as explained previously. Fixed scaffolds were rinsed with 1× PBS and transferred into either Anti-collagen Type-I FITC (1:5 (v/v)) or DAPI (1:1000 (v/v)) solutions in PBS. Scaffolds were incubated in Anti-collagen Type-I FITC solution at +4 °C overnight, and in DAPI solution at RT, 10 mins. After the incubation period, scaffolds were rinsed in 1× PBS prior to fluorescent microscope analysis (Zeiss Observer Z1).

2.5. Statistical analysis

Cell viability and proliferation analyses were done by using 6 independent experimental data sets and expressed as mean value ±SD. Mixed ANOVA was performed by SPSS 22.0. Post-hoc analysis was performed with LSD correction for pairwise comparisons. The significance level was accepted as $p < 0.05$ at all analyses.

3. Results and discussion

3.1. Fabrication of QSH scaffold

The flowsheet of QSH extraction is illustrated in Fig. 1. Unprocessed QSH was obtained via conventional water extraction technique by immersing seeds in UP H_2O. Pre-gelation has occured at around 24 h, and has monitored by apparent viscosity technique [25]. Here, QSH exhibits condensed phase rather than viscous liquid prior to crosslinking, because of secondary interactions between the glucuronoxylan molecules, however, it tends to disintegrate by mechanical force and start flowing [40]. Therefore, this state is called as pre-gel. Transparent pre-gel was obtained after filtration of remaining seed particles as shown in Fig. 1. Pre-gel was lyophilized immediately after filtration. As shown in Fig. 1, non-transparent, sponge-like scaffolds were obtained after lyophilization process. Lyophilized pre-gels were then crosslinked with GTA to obtain non-soluble scaffold materials for further cell culture studies. 2 mg mL^{-1} QSH concentration was decided as optimum concentration parameter due to handling of pre-gels; higher concentrations resulted in brittle texture, which is an undesirable property for tissue scaffolds.

3.2. Morphological characterization of QSH scaffold

More detailed characterization and morphological investigation were performed by SEM. As shown in Fig. 2, all non-crosslinked, lightly crosslinked and heavily crosslinked QSH have porous and interconnected structure, which is quite similar to majorly used scaffolds in tissue engineering; such as collagen [41]. As depicted in Fig. 2c, average pore size of non-crosslinked QSH samples was around 99.85 μm while 22.52% porosity was obtained. After crosslinking of QSH, average pore size decreased to 76.59 μm and 18.36% porosity was obtained for lightly crosslinked sample (Fig. 2f). For heavily crosslinked samples, average pore size decreased to 56.04 μm while 13.58% porosity was obtained (Fig. 2i). With the increased degree of crosslinking, the QSH scaffold gained a firmer structure, which resulted in a decrease in interconnected pore size and porosity [37]. Interconnected and porous structure is a fundamental issue in scaffold design [42] and QSH provides high porosity that promises high potential in tissue engineering.

Fig. 2j shows cross-section of QSH demonstrating the edge morphology of lyophilized QSHs that exhibit stacked layer formation. The smoother topography shown by the outer layers, which may be a consequence of homogeneous drying, on the other hand, inner layers show sponge like morphology due to inhomogeneous water removal during freeze-drying process. Stacked layers ascertain that building blocks of QSH exhibiting mutual interactions with water molecules throughout secondary forces. In particular, hydrogen bonding between water and

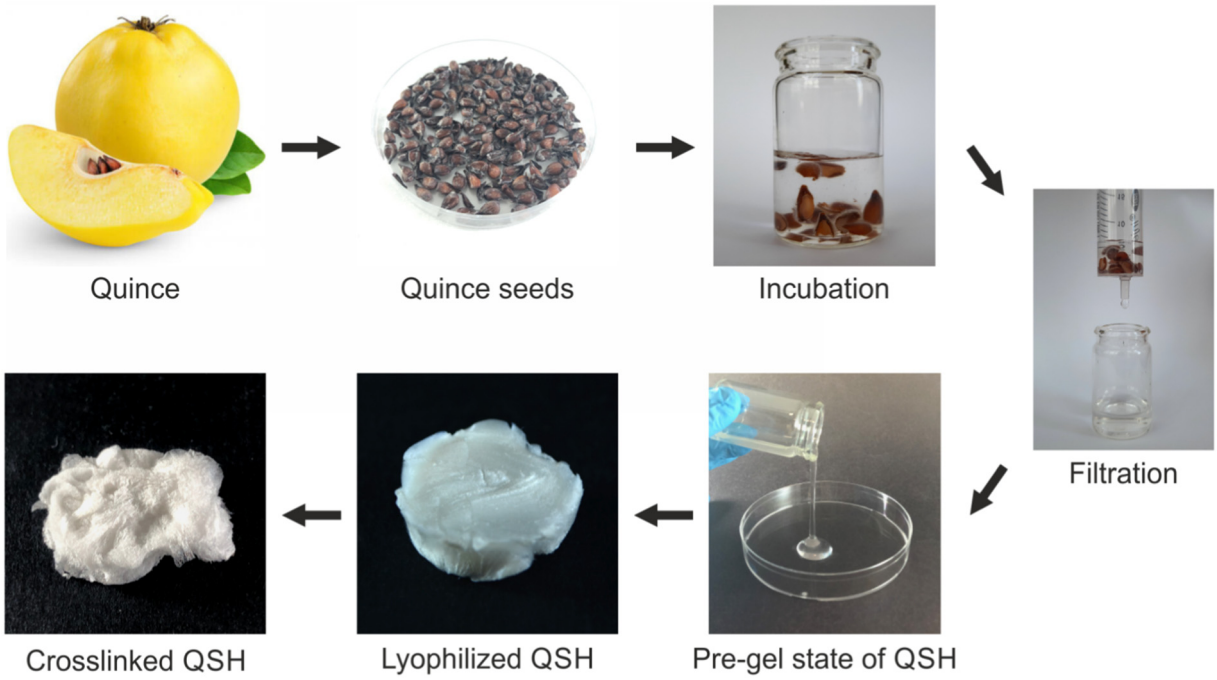

Fig. 1. Schematic illustration of QSH extraction and scaffold fabrication process.

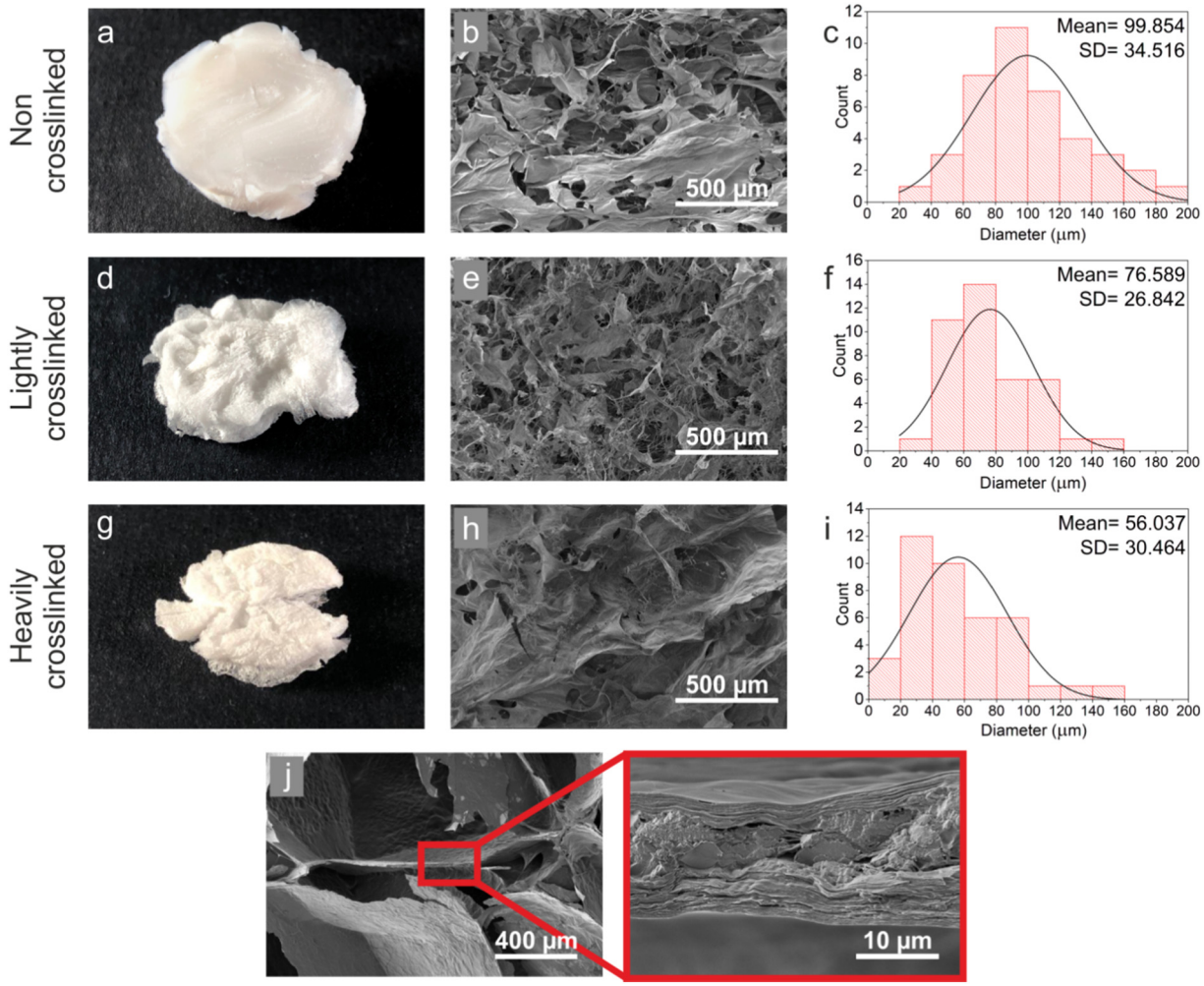

Fig. 2. Characterization of QSH scaffolds; (a,d,g)macro images of QSH for (a)non-crosslinked, (d)lightly crosslinked and (g)heavily crosslinked form, (b,e,h) SEM images of porous QSHs for (b)non-crosslinked, (e)lightly crosslinked and (h)heavily crosslinked form (scale bar = 500 μm), (c,f,i) average pore size distribution histograms of QSH for (c)non-crosslinked, (f) lightly crosslinked and (i)heavily crosslinked form, (j)cross-sectional SEM photos of QSH, (scale bars = 400 μm and 10 μm respectively).

QSH may play role in gelation and condensation of layers. We consider that stacked layers may eventually contribute to the mechanical properties of the gel.

3.3. Morphological and mechanical analysis of QSH scaffold via AFM

Morphology of non-crosslinked (Fig. 3a) and crosslinked (Fig. 3d) QSH samples are analyzed by AFM measurements. Height profiles of the corresponding lines drawn in Fig. 3a and d were illustrated in Fig. 3b and e, respectively. The surface roughness of non-crosslinked and crosslinked samples was calculated as 613.5 nm and 2 μm, respectively. It is evident that the surface roughness increased about 3.5 times after the crosslinking process. Young's modulus distributions before and after crosslinking of QSH samples were shown in Fig. 3c and f. The Young's modulus of non-crosslinked QSH was found to be 53 MPa while crosslinked QSH sample was 76 MPa. The increase was expected due to chemical crosslinking [43–45] process since it provides more entanglement in polymer chains. As reported earlier, the chain entanglements mediate energy dissipation [43–45]. Non-crosslinked QSH (Fig. 3c) showed heterogeneous distribution of Young's modulus ranging between 12 MPa (blue regions) to 60 MPa (green regions) whereas crosslinked one (Fig. 3f) exhibited more homogenous Young's modulus distribution with 70 MPa to 80 MPa (green regions). The increase in the Young's modulus caused by the crosslinking, indicating that the material has a more rigid structure, which was shown by AFM measurements.

3.4. Analysis of QSH content and crosslinking efficiency

ATR-FTIR spectroscopy was used to identify the major functional groups in QSH structure and also degree of crosslinking was analyzed. GTA based crosslinking relies on the basis of aldehyde-hydroxyl group bonding. Dialdehyde groups of GTA yield strong bonds with hydroxyl groups of QSH [46]. Spectrums of non-crosslinked, lightly crosslinked (0.03 M GTA), and heavily crosslinked (0.5 M GTA) QSHs are presented in Fig. 4. The broad band that appeared between 3600 and 3000 cm^{-1} is the characteristic stretching peak of hydrogen bonding involving the hydroxyl groups of QSH [11,25,28]. A rather intense peak was observed around this area in non-crosslinked QSH compared to crosslinked QSHs, which is attributed to intra/inter hydrogen bonds formed between hydroxyl groups of QSH and CHO groups of GTA [46,47]. Weak CH stretching vibration peaks are observed between 2800 and 2950 cm^{-1} from CH and CH_2 in cellulose and hemicellulose components [11,25,48]. Characteristic peaks around 1598 and 1420 cm^{-1} show the presence of COO^- asymmetric stretching carbonyl group (C=O) and COO^- symmetric stretching that indicates carbonyl (C=O) and carboxyl groups in the structure shows the presence of uronic acid [38,49–52]. Also, band at 1730 cm^{-1} suggests the existence of grafting [12] or esterification in carboxylic group [25,28,35].

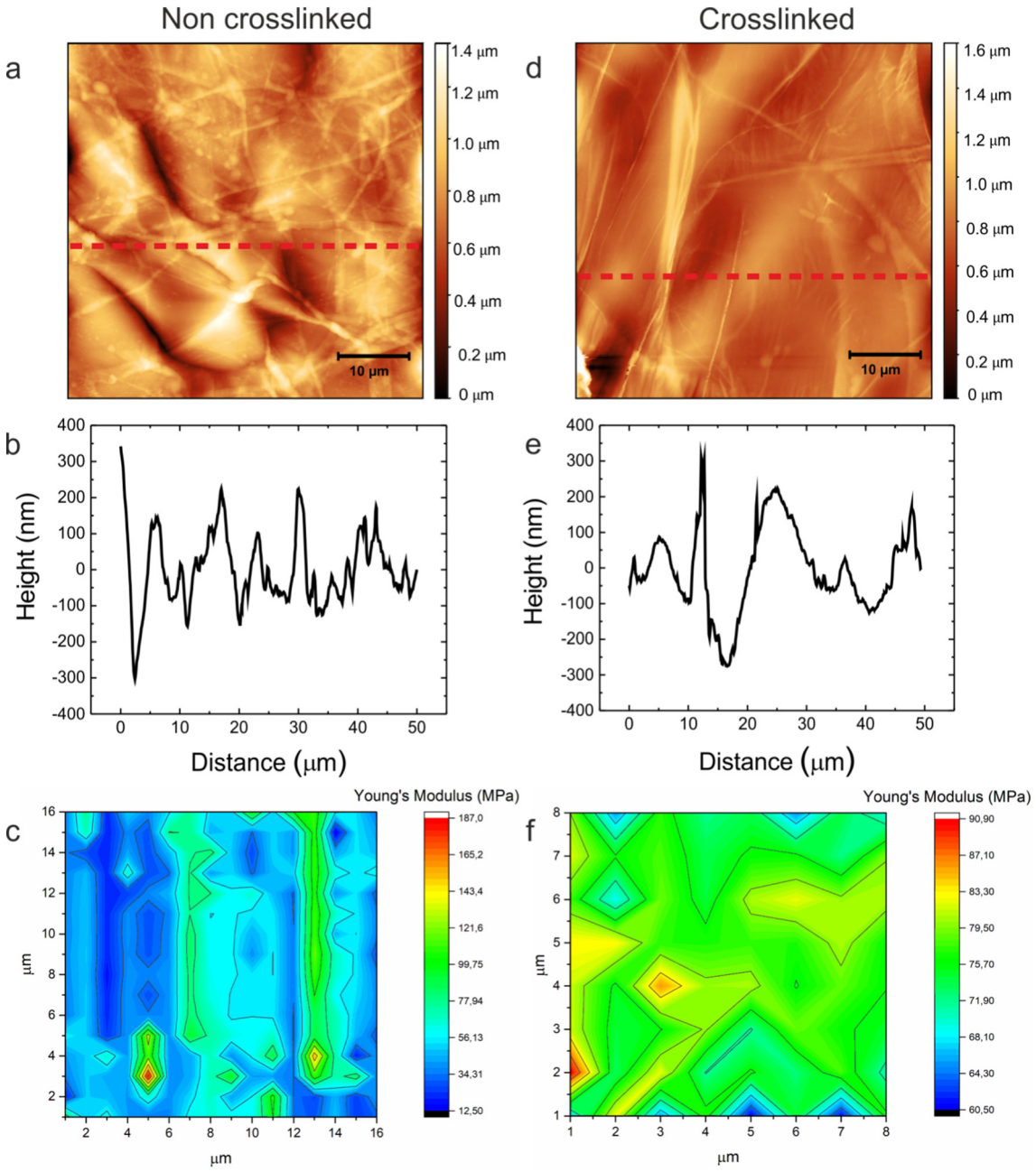

Fig. 3. AFM analysis showing the surface characteristics of QSH (a) surface topography, (b) height profile and (c) force-distance profile of non-crosslinked and (d) surface topography, (e) height profile and (f) force-distance profile of crosslinked QSH scaffolds.

Also, an increased peak around 1730 cm^{-1} can be referred to as the acetate bridge through combining the dialdehyde of GTA and hydroxyl group of cellulose content of QSH with the catalyzing of hydrochloric acid [46,53,54]. Typical polysaccharide bands are exhibited in the range of 1200–1000 cm^{-1} assigned to C-OH bending and C-O-C stretching of glycosidic linkage [48–50,55]. Overall FTIR results indicate that crosslinking of QSH was accomplished successfully by using GTA.

3.5. Swelling behavior of QSH

Swelling capacity of QSH is illustrated in Fig. 5a. In general, all QSH samples; both lightly and heavily crosslinked ones, reached equilibrium swelling within 2 h while no deswelling was observed. Higher swelling was observed for lightly crosslinked QSH, while lower swelling was observed for heavily crosslinked QSH. As expected, degree of crosslinking affects the swelling capacity of QSH; where highly porous structure enhance the swelling behavior compared to the less porous one [37,56,57].

3.6. Protein adsorption assessment of QSH scaffold

Protein-scaffold interaction indicates adhesion potential of cells onto a scaffold. Here protein adsorption analysis was done to investigate capability of QSH as a scaffold material. Protein adsorption profiles are shown in Fig. 5b for adsorbed BSA on QSH. Amount of adsorbed protein reached an equilibrium at 1000 μg mL^{-1} stock concentration and total adsorbed protein amount was around

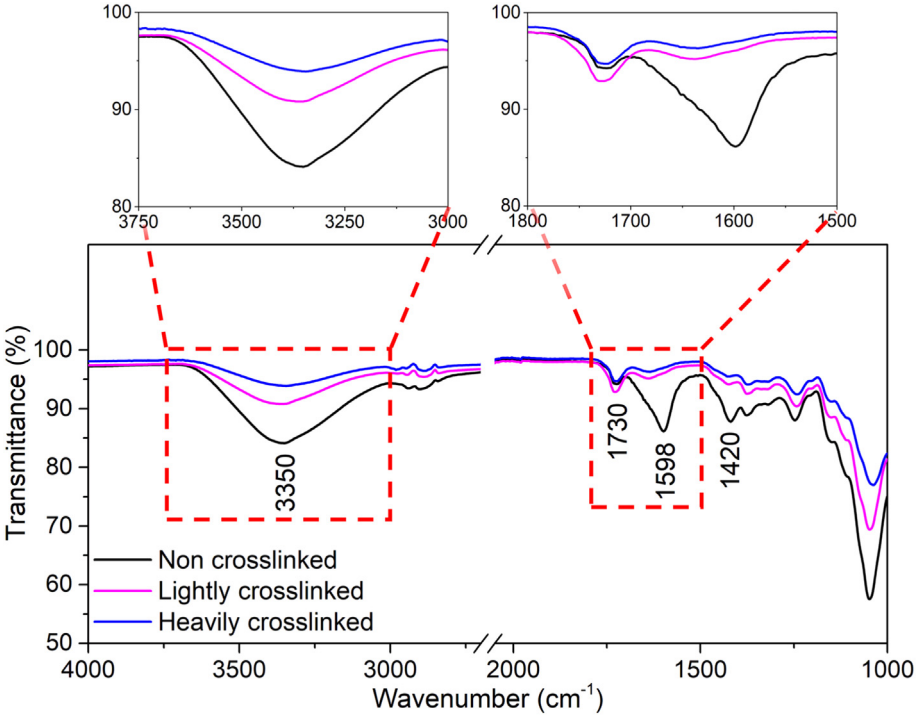

Fig. 4. FTIR spectrum of non-crosslinked, lightly crosslinked and heavily crosslinked QSH scaffolds.

143 μg mL^{-1} indicating maximum protein holding capacity of QSH. This indicates that QSH has a certain protein holding capacity; therefore, it also favors cellular adhesion and cell proliferation.

3.7. 3D cell culture studies

Cell proliferation and viability analyses were done to investigate biocompatibility of QSH scaffold. Cell viability profiles are shown against crosslinking in Fig. 6a, and against cell number in Fig. 6b. As shown in Fig. 6a, NIH-3T3 fibroblast cells were proliferated faster on lightly crosslinked QSH than heavily crosslinked one, which can be attributed to more porous structure of the lightly crosslinked scaffold. In addition, higher GTA concentration (0.5 M) in heavily crosslinked QSH could have a negative effect on cell viability. Therefore, lightly crosslinked QSH was used for further cellular studies. For cell number evaluation, low density (2×10^5) and high density (2×10^6) NIH-3T3 cells were seeded on QSH (Fig. 6b). In all sets, proliferation of control groups (TCPS) was limited because of the insufficient surface area. High density cell seeding provided higher proliferation rate and higher viability because of increased cell number in unit area increased supported the cell-cell interactions, therefore cell proliferation is increased [58]. Moreover, long-term cell culturing (Fig. 6c) was done to examine the cellular growth in long term. As expected, cell proliferation decreased in TCPS controls due to limited surface area, and cells started to die after day 9. Cell-material interaction is an important parameter in terms of biocompatibility of a material [58]. In contrary to standard 2D cell culture, 3D scaffold provided a suitable microenvironment and surface area for increased cell proliferation, although proliferation rate is slower due to cell adhesion and adaptation period, cell proliferation on QSH increased gradually during 15-day culturing (Fig. 6c).

Furthermore, cell viability was analyzed through Live/Dead assay for TCPS (Fig. 7a), lightly crosslinked QSH (Fig. 7b) and heavily crosslinked QSH (Fig. 7c). Starting from day 1 NIH-3T3 fibroblast cells started to form aggregates, which are early forms of spheroids, and spheroid formation was clearly observed in both QSH scaffolds (Fig. 7b and c) starting from day 3 onwards. However, cell viability and total number of spheroids were lower on heavily crosslinked QSH compared to lightly crosslinked one. As parallel to the literature [59], higher GTA concentrations had toxic effect on cells. In addition, QSH scaffolds were compared with TCPS in terms of viability and it was observed that limited culture area in 2D environment (TCPS) resulted in contact inhibition and cells started to die starting from day 3.

3.8. ECM analysis

For a successful tissue engineering application, it is required that cells produce and secrete their own ECM components. Here, inter/intracellular components for long-term (2 months) cell culture samples were evaluated via SEM (Fig. 8a) and immunostaining methodologies (Fig. 8b and c). As depicted in Fig. 8a, spheroids were homogeneously scattered inside the QSH where average spheroid diameter was around 300 μm. As shown in Fig. 8b, nuclear DAPI staining was done to investigate cellular entities inside the spheroid structure. DAPI staining results also confirm the homogeneous distribution of cells inside the spheroids.

In order to investigate ECM production, collagen secretion was analyzed for 2-month old samples when the secretion rate was the highest [60,61]. Collagen secretion during spheroid formation has been examined by Anti-collagen Type-I FITC staining. After collagen immunostaining, observed fluorescence images (Fig. 8c) confirmed the presence of collagen Type-I secreted by NIH-3T3 cells, and exhibited similar spheroid patterns with SEM and DAPI analyses.

4. Conclusion

Biomaterial potency of QSH as a scaffold material for tissue engineering was extensively examined in this paper. QSH was evaluated in terms

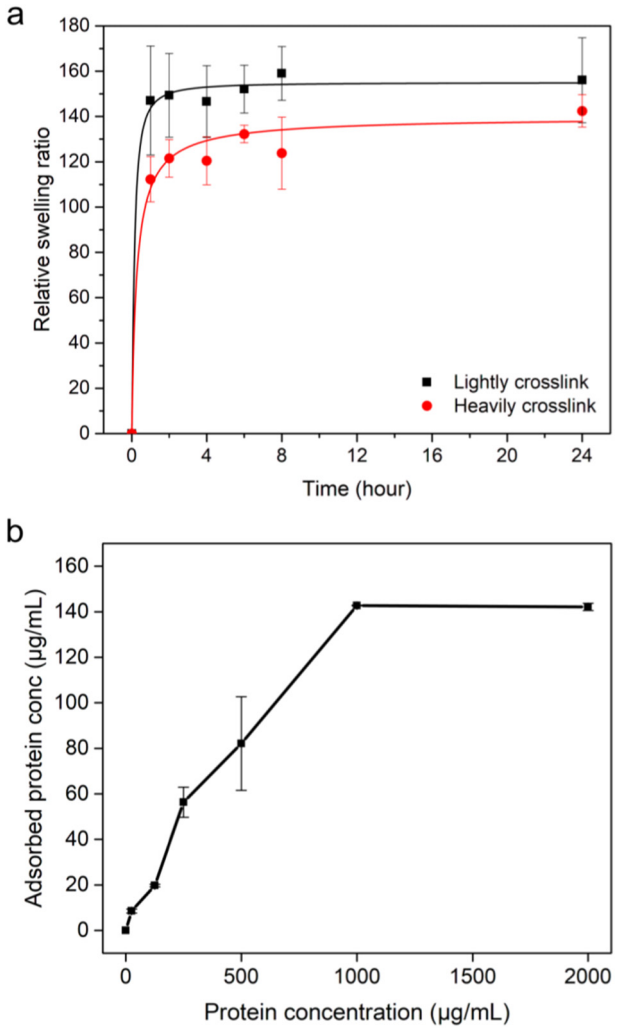

Fig. 5. (a) Swelling ratio of QSH. Data are shown for 1, 2, 4, 6, 8 and 24 h, (b) Protein adsorption profile of QSH.

of porosity, crosslinking properties, swelling ratio and protein adsorption, and NIH-3T3 fibroblast cells were cultured in 3D microenvironment to observe biocompatibility. Highly porous scaffold was obtained from 2 mg mL^{-1} lyophilized QSH and it was crosslinked by GTA where degree of crosslinking was adjusted by varying the GTA concentration; lightly crosslinked QSH was obtained with 0.03 M GTA and heavily crosslinked one was obtained with 0.5 M GTA. Biocompatibility of QSH was verified through cell viability, proliferation, and ECM secretion analyses. NIH-3T3 fibroblast cells in lightly crosslinked QSH showed improved viability and proliferation. Live/Dead analysis, SEM imaging and DAPI staining successfully demonstrated the spheroid formation in 3D microenvironment up to 2 months. Moreover, ECM formation was confirmed via Collagen secretion analysis. The overall results clearly prove that QSH is a novel scaffold material, which has suitable mechanical features, remarkable swelling capacity, as well as good biocompatibility, and it promotes tissue formation. The fabricated QSH potentially offers an efficient and cost-effective biomaterial for 3D cell culture and tissue engineering applications.

CRediT authorship contribution statement

Meltem Guzelgulgen: Investigation, Formal Analysis, Writing-Original Draft.

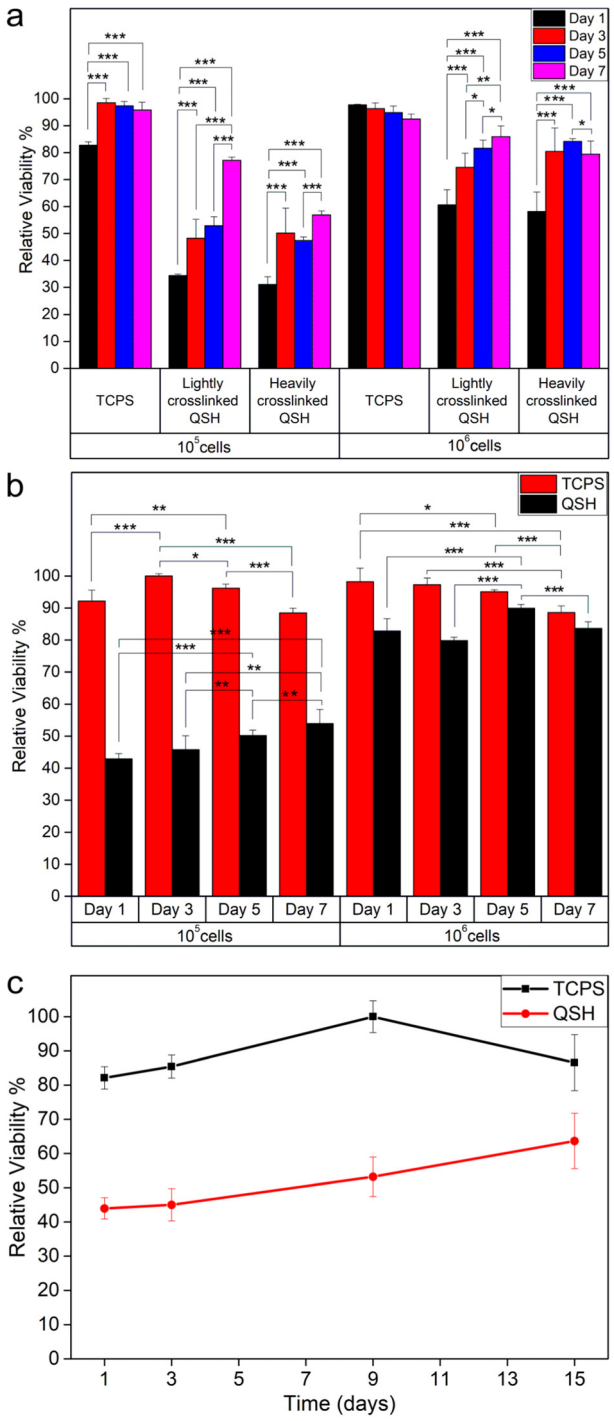

Fig. 6. Cell viability profiles of NIH-3T3 fibroblast cells on QSH scaffolds, evaluated by AlamarBlue assay (a) cell viability against crosslinking parameters, (b) cell viability against cell number, (n = 6) (statistical difference $^{*}p < 0.05$, $^{**}p < 0.01$, $^{***}p < 0.001$) (c) cell viability for long term culturing.

Dilce Kendir-Inanc: Investigation, Writing-Original Draft.

Umit Hakan Yildiz: Conceptualization, Supervision, Writing - Review & Editing.

Ahu Arslan-Yildiz: Conceptualization, Supervision, Writing - Review & Editing.

Funding

This research did not receive any specific grant from funding agencies in the public, commercial, or not-for-profit sectors.

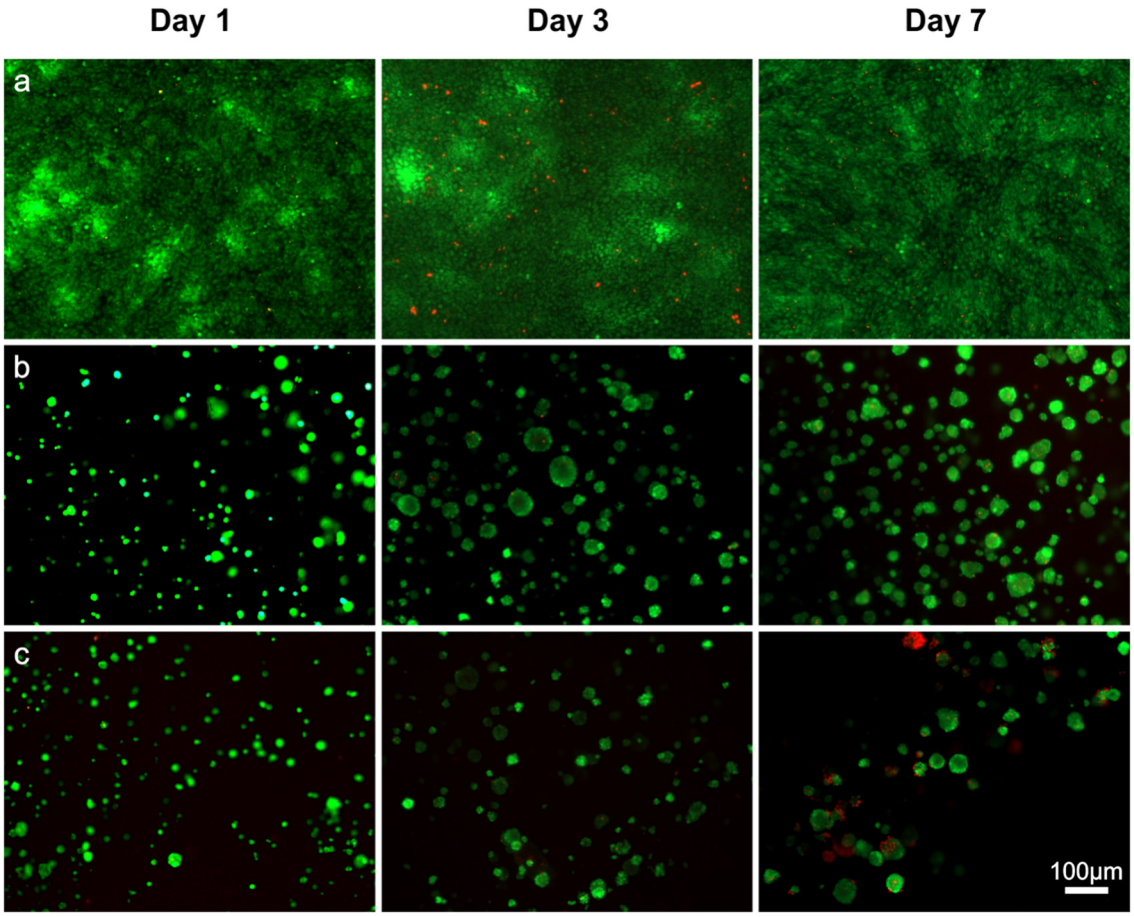

Fig. 7. Cell viability evaluation of NIH-3T3 fibroblast cells on QSH, evaluated by Live/Dead assay; (a) TCPS control group, (b) lightly crosslinked (0.03 M GTA) QSH, (c) heavily crosslinked (0.5 M GTA) QSH. (scale bar 100 μm).

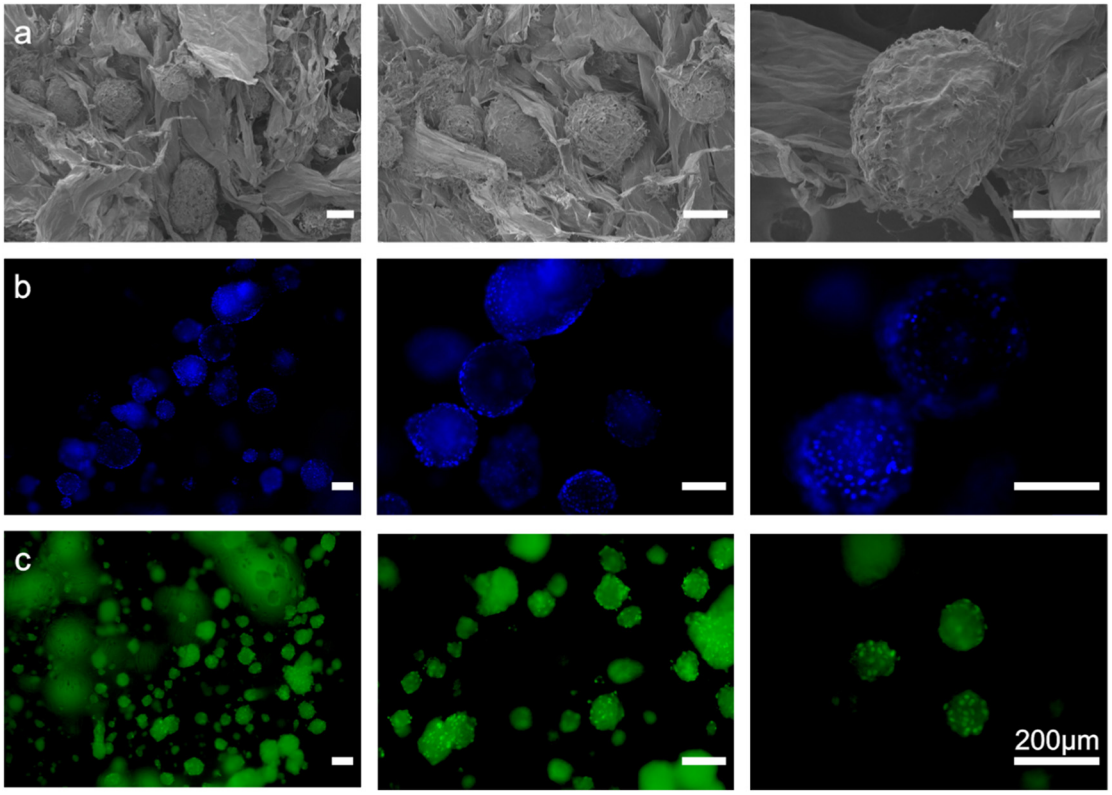

Fig. 8. Spheroid formations in QSH scaffolds (a) SEM images of QSH with cells, (b) DAPI staining and (c) Anti-collagen Type-I FITC staining (scale bars = 200 μm).

Acknowledgments

The authors acknowledge Izmir Institute of Technology; Biotechnology and Bioengineering Research and Application Center (IZTECH-BIOMER) and Center for Materials Research (IZTECH-MAM) for the instrumental facilities provided to accomplish this work.

References

[1] N.A. Peppas, J.Z. Hilt, A. Khademhosseini, R. Langer, Hydrogels in biology and medicine: from molecular principles to bionanotechnology, Adv. Mater. 18 (2006) 1345–1360, https://doi.org/10.1002/adma.200501612.
[2] K.Y. Lee, D.J. Mooney, Hydrogels for tissue engineering, Chem. Rev. 101 (2001) 1869–1880, https://doi.org/10.1021/cr000108x.
[3] M. Fenbo, L. Sijing, L.I. Ruiz-Ortega, Z. Yuanjun, X. Lei, W. Kui, L. Lijun, T. Bin, Effects of alginate/chondroitin sulfate-based hydrogels on bone defects healing, Mater. Sci. Eng. C 116 (2020), 111217, https://doi.org/10.1016/j.msec.2020.111217.
[4] W.S. Toh, X.J. Loh, Advances in hydrogel delivery systems for tissue regeneration, Mater. Sci. Eng. C 45 (2014) 690–697, https://doi.org/10.1016/j.msec.2014.04.026.
[5] S.M. Mihaila, A.K. Gaharwar, R.L. Reis, A.P. Marques, M.E. Gomes, A. Khademhosseini, Photocrosslinkable kappa-carrageenan hydrogels for tissue engineering applications, Adv. Healthcare Mater. 2 (2013) 895–907. https://doi.org/10.1002/adhm.201200317.
[6] P. Sensharma, G. Madhumathi, R.D. Jayant, A.K. Jaiswal, Biomaterials and cells for neural tissue engineering: current choices, Mater. Sci. Eng. C 77 (2017) 1302–1315, https://doi.org/10.1016/j.msec.2017.03.264.
[7] J. Liu, H. Chen, Y. Wang, G. Li, Z. Zheng, D.L. Kaplan, X. Wang, X. Wang, Flexible water-absorbing silk-fibroin biomaterial sponges with unique pore structure for tissue engineering, ACS Biomater. Sci. Eng. 6 (2020) 1641–1649, https://doi.org/10.1021/acsbiomaterials.9b01721.
[8] B. Köksal, S. Özenler, M. Yücel, U. Yildiz, A. Arslan Yildiz, Biomimetic and Synthetic Gels for Nanopharmaceutical Applications, 2021 273–309, https://doi.org/10.1007/978-3-030-44925-4_7.
[9] E. Türker, Ü.H. Yildiz, A. Arslan Yildiz, Biomimetic hybrid scaffold consisting of co-electrospun collagen and PLLCL for 3D cell culture, Int. J. Biol. Macromol. 139 (2019) 1054–1062, https://doi.org/10.1016/j.ijbiomac.2019.08.082.
[10] N. Celikkin, C. Rinoldi, M. Costantini, M. Trombetta, A. Rainer, W. Święszkowski, Naturally derived proteins and glycosaminoglycan scaffolds for tissue engineering applications, Mater. Sci. Eng. C 78 (2017) 1277–1299, https://doi.org/10.1016/j.msec.2017.04.016.
[11] F. Rezagholi, S.M.B. Hashemi, A. Gholamhosseinpour, M.H. Sherahi, M.A. Hesarinejad, M.T. Ale, Characterizations and rheological study of the purified polysaccharide extracted from quince seeds, J. Sci. Food Agric. 99 (2019) 143–151, https://doi.org/10.1002/jsfa.9155.
[12] M. Jouki, S.A. Mortazavi, F.T. Yazdi, A. Koocheki, Optimization of extraction, antioxidant activity and functional properties of quince seed mucilage by RSM, Int. J. Biol. Macromol. 66 (2014) 113–124, https://doi.org/10.1016/j.ijbiomac.2014.02.026.
[13] M. Jouki, F. Tabatabaei Yazdi, S.A. Mortazavi, A. Koocheki, Physical, barrier and antioxidant properties of a novel plasticized edible film from quince seed mucilage, Int. J. Biol. Macromol. 62 (2013) 500–507, https://doi.org/10.1016/j.ijbiomac.2013.09.031.
[14] H. Deng, J. Sun, Z. Yu, Z. Guo, C. Xu, Low-intensity near-infrared light-triggered spatiotemporal antibiotics release and hyperthermia by natural polysaccharide-based hybrid hydrogel for synergistic wound disinfection, Mater. Sci. Eng. C (2020) 111530, https://doi.org/10.1016/j.msec.2020.111530.
[15] V.D. Prajapati, G.K. Jani, N.G. Moradiya, N.P. Randeria, Pharmaceutical applications of various natural gums, mucilages and their modified forms, Carbohydr. Polym. 92 (2013) 1685–1699, https://doi.org/10.1016/j.carbpol.2012.11.021.
[16] A.A. Hemmati, H. Kalantari, A. Jalali, S. Rezai, H.H. Zadeh, Healing effect of quince seed mucilage on T-2 toxin-induced dermal toxicity in rabbit, Exp. Toxicol. Pathol. 64 (2012) 181–186, https://doi.org/10.1016/j.etp.2010.08.004.
[17] L.R. Stevens, K.J. Gilmore, G.G. Wallace, M. in het Panhuis, Tissue engineering with gellan gum, Biomater. Sci. 4 (2016) 1276–1290, https://doi.org/10.1039/C6BM00322B.
[18] P.S. Gungor-Ozkerim, I. Inci, Y.S. Zhang, A. Khademhosseini, M.R. Dokmeci, Bioinks for 3D bioprinting: an overview, Biomater. Sci. 6 (2018) 915–946, https://doi.org/10.1039/C7BM00765E.
[19] J.L. Drury, D.J. Mooney, Hydrogels for tissue engineering: scaffold design variables and applications, Biomaterials 24 (2003) 4337–4351, https://doi.org/10.1016/S0142-9612(03)00340-5.
[20] A.D. Augst, H.J. Kong, D.J. Mooney, Alginate hydrogels as biomaterials, Macromol. Biosci. 6 (2006) 623–633, https://doi.org/10.1002/mabi.200600069.
[21] A. Svensson, E. Nicklasson, T. Harrah, B. Panilaitis, D.L. Kaplan, M. Brittberg, P. Gatenholm, Bacterial cellulose as a potential scaffold for tissue engineering of cartilage, Biomaterials 26 (2005) 419–431, https://doi.org/10.1016/j.biomaterials.2004.02.049.
[22] G. Kogan, L. Šoltés, R. Stern, P. Gemeiner, Hyaluronic acid: a natural biopolymer with a broad range of biomedical and industrial applications, Biotechnol. Lett. 29 (2006) 17–25, https://doi.org/10.1007/s10529-006-9219-z.
[23] C. Guyot, M. Cerruti, S. Lerouge, Injectable, strong and bioadhesive catechol-chitosan hydrogels physically crosslinked using sodium bicarbonate, Mater. Sci. Eng. C (2020) 111529, https://doi.org/10.1016/j.msec.2020.111529.
[24] B. Abbastabar, M.H. Azizi, A. Adnani, S. Abbasi, Determining and modeling rheological characteristics of quince seed gum, Food Hydrocoll. 43 (2015) 259–264, https://doi.org/10.1016/j.foodhyd.2014.05.026.
[25] L. Wang, H.-M. Liu, A.-J. Xie, X.-D. Wang, C.-Y. Zhu, G.-Y. Qin, Chinese quince (Chaenomeles sinensis) seed gum: structural characterization, Food Hydrocoll. 75 (2018) 237–245, https://doi.org/10.1016/j.foodhyd.2017.08.001.
[26] M.R. Vignon, C. Gey, Isolation, 1H and 13C NMR studies of (4-O-methyl-d-glucurono)-d-xylans from luffa fruit fibres, jute bast fibres and mucilage of quince tree seeds, Carbohydr. Res. 307 (1998) 107–111, https://doi.org/10.1016/S0008-6215(98)00002-0.
[27] M.U. Ashraf, M.A. Hussain, G. Muhammad, M.T. Haseeb, S. Bashir, S.Z. Hussain, I. Hussain, A superporous and superabsorbent glucuronoxylan hydrogel from quince (Cydonia oblanga): stimuli responsive swelling, on-off switching and drug release, Int. J. Biol. Macromol. 95 (2017) 138–144, https://doi.org/10.1016/j.ijbiomac.2016.11.057.
[28] M.U. Ashraf, M.A. Hussain, S. Bashir, M.T. Haseeb, Z. Hussain, Quince seed hydrogel (glucuronoxylan): evaluation of stimuli responsive sustained release oral drug delivery system and biomedical properties, J. Drug Deliv. Sci. Technol. 45 (2018) 455–465. doi:https://doi.org/10.1016/j.jddst.2018.04.008.
[29] L. Wang, M. Wu, H.-M. Liu, Y.-X. Ma, X.-D. Wang, G.-Y. Qin, Subcritical fluid extraction of Chinese quince seed: optimization and product characterization, Molecules 22 (2017) 528, https://doi.org/10.3390/molecules22040528.
[30] G. Sworn, S. Kasapis, Effect of conformation and molecular weight of co-solute on the mechanical properties of gellan gum gels, Food Hydrocoll. 12 (1998) 283–290, https://doi.org/10.1016/s0268-005x(98)00016-2.
[31] Y. Viturawong, P. Achayuthakan, M. Suphantharika, Gelatinization and rheological properties of rice starch/xanthan mixtures: effects of molecular weight of xanthan and different salts, Food Chem. 111 (2008) 106–114, https://doi.org/10.1016/j.foodchem.2008.03.041.
[32] H.A. Khouryieh, T.J. Herald, F. Aramouni, S. Alavi, Intrinsic viscosity and viscoelastic properties of xanthan/guar mixtures in dilute solutions: effect of salt concentration on the polymer interactions, Food Res. Int. 40 (2007) 883–893, https://doi.org/10.1016/j.foodres.2007.03.001.
[33] J.L. Doublier, B. Launay, Rheology of galactomannan solutions: comparative study of guar gum and locust bean gum, J. Texture Stud. 12 (1981) 151–172, https://doi.org/10.1111/j.1745-4603.1981.tb01229.x.
[34] L. Wang, H.-M. Liu, C.-Y. Zhu, A.-J. Xie, B.-J. Ma, P.-Z. Zhang, Chinese quince seed gum: flow behaviour, thixotropy and viscoelasticity, Carbohydr. Polym. 209 (2019) 230–238, https://doi.org/10.1016/j.carbpol.2018.12.101.
[35] L. Wang, H.-M. Liu, G.-Y. Qin, Structure characterization and antioxidant activity of polysaccharides from Chinese quince seed meal, Food Chem. 234 (2017) 314–322, https://doi.org/10.1016/j.foodchem.2017.05.002.
[36] M. Lawrence, Y. Jiang, Porosity, Pore Size Distribution, Micro-Structure, Springer, Netherlands, 2017 39–71, https://doi.org/10.1007/978-94-024-1031-0_2.
[37] H. Chavda, C. Patel, Effect of crosslinker concentration on characteristics of superporous hydrogel, Int. J. Pharm. Investig. 1 (2011) 17–21, https://doi.org/10.4103/2230-973X.76724.
[38] A.-J. Xie, H.-S. Yin, H.-M. Liu, C.-Y. Zhu, Y.-J. Yang, Chinese quince seed gum and poly (N,N -diethylacryl amide-co-methacrylic acid) based pH-sensitive hydrogel for use in drug delivery, Carbohydr. Polym. 185 (2018) 96–104, https://doi.org/10.1016/j.carbpol.2018.01.007.
[39] M. Kim, Y.-J. Kim, K. Gwon, G. Tae, Modulation of cell adhesion of heparin-based hydrogel by efficient physisorption of adhesive proteins, Macromol. Res. 20 (2012) 271–276, https://doi.org/10.1007/s13233-012-0058-6.
[40] B. Koksal, R. Onbas, M. Baskurt, H. Sahın, A. Arslan Yildiz, U.H. Yildiz, Boosting up printability of biomacromolecule based bio-ink by modulation of hydrogen bonding pairs, Eur. Polym. J. 141 (2020) 110070. doi:doi:https://doi.org/10.1016/j.eurpolymj.2020.110070.
[41] D.A. Wahl, E. Sachlos, C. Liu, J.T. Czernuszka, Controlling the processing of collagen-hydroxyapatite scaffolds for bone tissue engineering, J. Mater. Sci. Mater. Med. 18 (2007) 201–209, https://doi.org/10.1007/s10856-006-0682-9.
[42] L. Moroni, J.R. de Wijn, C.A. van Blitterswijk, 3D fiber-deposited scaffolds for tissue engineering: influence of pores geometry and architecture on dynamic mechanical properties, Biomaterials 27 (2006) 974–985, https://doi.org/10.1016/j.biomaterials.2005.07.023.
[43] S. Suto, M. Yoshinaka, Chemical cross-linking of cholesteric liquid-crystalline hydroxypropyl cellulose with dialdehydes, J. Mater. Sci. 28 (1993) 4644–4650, https://doi.org/10.1007/bf00414253.
[44] K. PourAkbar Saffar, A.R. Arshi, N. JamilPour, A.R. Najafi, G. Rouhi, L. Sudak, A cross-linking model for estimating Young's modulus of artificial bone tissue grown on carbon nanotube scaffold, J. Biomed. Mater. Res. A 94A (2010) 594–602, https://doi.org/10.1002/jbm.a.32737.
[45] O. Jeon, S.J. Song, K.-J. Lee, M.H. Park, S.-H. Lee, S.K. Hahn, S. Kim, B.-S. Kim, Mechanical properties and degradation behaviors of hyaluronic acid hydrogels cross-linked at various cross-linking densities, Carbohydr. Polym. 70 (2007) 251–257, https://doi.org/10.1016/j.carbpol.2007.04.002.
[46] H.S. Mansur, C.M. Sadahira, A.N. Souza, A.A.P. Mansur, FTIR spectroscopy characterization of poly (vinyl alcohol) hydrogel with different hydrolysis degree and chemically crosslinked with glutaraldehyde, Mater. Sci. Eng. C 28 (2008) 539–548, https://doi.org/10.1016/j.msec.2007.10.088.
[47] R. Rahmi, Comparative adsorption of Fe(III) and Cd(II) ions on glutaraldehyde crosslinked chitosan–coated cristobalite, Orient. J. Chem. 31 (2015) 2071–2076, https://doi.org/10.13005/ojc/310427.
[48] G. Archana, K. Sabina, S. Babuskin, K. Radhakrishnan, M.A. Fayidh, P.A.S. Babu, M. Sivarajan, M. Sukumar, Preparation and characterization of mucilage polysaccharide for biomedical applications, Carbohydr. Polym. 98 (2013) 89–94, https://doi.org/10.1016/j.carbpol.2013.04.062.
[49] W. Cai, H. Xu, L. Xie, J. Sun, T. Sun, X. Wu, Q. Fu, Purification, characterization and in vitro anticoagulant activity of polysaccharides from Gentiana scabra Bunge

roots, Carbohydr. Polym. 140 (2016) 308–313, https://doi.org/10.1016/j.carbpol.2015.12.054.
[50] G.D. Manrique, F.M. Lajolo, FT-IR spectroscopy as a tool for measuring degree of methyl esterification in pectins isolated from ripening papaya fruit, Postharvest Biol. Technol. 25 (2002) 99–107, https://doi.org/10.1016/S0925-5214(01)00160-0.
[51] H. Hosseinzadeh, S. Mohammadi, Quince seed mucilage magnetic nanocomposites as novel bioadsorbents for efficient removal of cationic dyes from aqueous solutions, Carbohydr. Polym. 134 (2015) 213–221, https://doi.org/10.1016/j.carbpol.2015.08.008.
[52] S.M.A. Razavi, S.W. Cui, Q. Guo, H. Ding, Some physicochemical properties of sage (Salvia macrosiphon) seed gum, Food Hydrocoll.. 35 (2014) 453–462. doi:doi:https://doi.org/10.1016/j.foodhyd.2013.06.022.
[53] S. Rimdusit, K. Somsaeng, P. Kewsuwan, C. Jubsilp, S. Tiptipakorn, Comparison of gamma radiation crosslinking and chemical crosslinking on properties of methylcellulose hydrogel, Eng. J. 16 (2012) 15–28, https://doi.org/10.4186/ej.2012.16.4.15.
[54] H. Zhu, B.B. Narakathu, Z. Fang, A. Tausif Aijazi, M. Joyce, M. Atashbar, L. Hu, A gravure printed antenna on shape-stable transparent nanopaper, Nanoscale 6 (2014) 9110, https://doi.org/10.1039/c4nr02036g.
[55] C. Ritzoulis, E. Marini, A. Aslanidou, N. Georgiadis, P.D. Karayannakidis, C. Koukiotis, A. Filotheou, S. Lousinian, E. Tzimpilis, Hydrocolloids from quince seed: extraction, characterization, and study of their emulsifying/stabilizing capacity, Food Hydrocoll. 42 (2014) 178–186, https://doi.org/10.1016/j.foodhyd.2014.03.031.
[56] C.G.D. Kruif, S.G. Anema, C. Zhu, P. Havea, C. Coker, Water holding capacity and swelling of casein hydrogels, Food Hydrocoll.. 44 (2015) 372–379. doi:https://doi.org/10.1016/j.foodhyd.2014.10.007.
[57] O. Okay, General properties of hydrogels, in: Gerald Gerlach, Karl-Friedrich Arndt (Eds.), Hydrogel Sensors and Actuators: Engineering and Technology, Springer Berlin Heidelberg, Berlin, Heidelberg 2009, pp. 1–14, https://doi.org/10.1007/978-3-540-75645-3_1.
[58] X. Yao, R. Peng, J. Ding, Cell–material interactions revealed via material techniques of surface patterning, Adv. Mater. 25 (2013) 5257–5286. doi:https://doi.org/10.1002/adma.201301762.
[59] S. Gao, Z. Yuan, W. Guo, M. Chen, S. Liu, T. Xi, Q. Guo, Comparison of glutaraldehyde and carbodiimides to crosslink tissue engineering scaffolds fabricated by decellularized porcine menisci, Mater. Sci. Eng. C 71 (2017) 891–900, https://doi.org/10.1016/j.msec.2016.10.074.
[60] Y. Dong, T. Yong, S. Liao, C.K. Chan, S. Ramakrishna, Long-term viability of coronary artery smooth muscle cells on poly(l -lactide- co -ϵ-caprolactone) nanofibrous scaffold indicates its potential for blood vessel tissue engineering, J. R. Soc. Interface 5 (2008) 1109–1118, https://doi.org/10.1098/rsif.2007.1354.
[61] D.L. Kusindarta, H. Wihadmadyatami, The Role of Extracellular Matrix in Tissue Regeneration, InTech, 2018https://doi.org/10.5772/intechopen.75728.